Numerical blood flow simulation in surgical corrections: what do we need for an accurate analysis?

Gregory Arbia, MS,[a,b] Chiara Corsini, MS,[c] Mahdi Esmaily Moghadam, MS,[d] Alison L. Marsden, PhD,[d] Francesco Migliavacca, PhD,[c] Giancarlo Pennati, PhD,[c] Tain-Yen Hsia, MD,[e] and Irene E. Vignon-Clementel, PhD,[a,b,] for the Modeling Of Congenital Hearts Alliance (MOCHA) Investigators[1]*

[a] *INRIA Paris-Rocquencourt, Le Chesnay Cedex, France*
[b] *UPMC Univ Paris 6, Laboratoire Jacques-Louis Lions, Paris, France*
[c] *Laboratory of Biological Structure Mechanics, Chemistry, Materials and Chemical Engineering Department "Giulio Natta", Politecnico di Milano, Milan, Italy*
[d] *Department of Mechanical and Aerospace Engineering, University of California San Diego, San Diego, California*
[e] *Cardiorespiratory Unit, Great Ormond Street Hospital for Children and UCL Institute of Cardiovascular Science, London, UK*

Article history:
Received 30 April 2013
Received in revised form
17 July 2013
Accepted 18 July 2013
Available online 11 August 2013

* *Corresponding author*. REO team-project, INRIA Paris-Rocquencourt, bat 16, BP 105, 78153 Le Chesnay Cedex, France. Tel.: +33 139 63 5118; fax +33 139 63 5082.
E-mail address: vie@stanfordalumni.org (I.E. Vignon-Clementel).

[1] MOCHA Investigators: Andrew Taylor, MD, Alessandro Giardini, MD, Sachin Khambadkone, MD, Silvia Schievano, PhD, Marc de Leval, MD, and T.-Y. Hsia, MD (Institute of Cardiovascular Sciences, UCL, London, UK); Edward Bove, MD, and Adam Dorfman, MD (University of Michigan, Ann Arbor, MI, USA); G. Hamilton Baker, MD, and Anthony Hlavacek (Medical University of South Carolina, Charleston, SC, USA); Francesco Migliavacca, PhD, Giancarlo Pennati, PhD, and Gabriele Dubini, PhD (Politecnico di Milano, Milan, Italy); Alison Marsden, PhD (University of California, San Diego, CA, USA); Jeffrey Feinstein, MD (Stanford University, Stanford, CA, USA); Irene Vignon-Clementel (INRIA, Paris-Rocquencourt, France); Richard Figliola, PhD, and John McGregor, PhD (Clemson University, Clemson, SC, USA).

1. Introduction

Computational fluid dynamics (CFD) has been increasingly used in cardiovascular research to model how hemodynamics change due to a pathology (see, e.g., [1–4]), predict hemodynamic changes due to surgical repair [5,6], explore different scenarios for treatment (see, e.g., [7–10]), plan therapy [11], for example by noninvasively computing indices that are otherwise invasively measured such as fractional flow reserve [12], and design artificial devices or conduits that are subject to stress and pressure from blood flow (see, e.g., [13–15]).

The Food and Drug Administration is integrating computational modeling into its evaluation and testing processes with increasing frequency and mandate [16]. Commercially developed numerical codes have increased the availability of such tools to a wider range of research, design, and clinical users. In parallel but independently, a number of research-specific codes have been developed, some of which have been made available as open sources. A few studies or "simulation challenges" have thus now emerged to compare codes or simulation approaches [17–20] to ascertain the validity and accuracy of these various codes.

To achieve effective solution, there are several necessary steps to numerically simulate blood flow: geometrical mesh generation from image data, choice of boundary conditions for the blood flow equations, and choice of numerical algorithm to compute the pressure and flow solution. These steps will be defined in the Methods section. Any misstep or inaccurate performance along the simulation algorithm can lead to erroneous results and potentially misleading conclusions. Therefore, we sought to systematically examine the choices of each of these step to assess whether the choice of solver code remains an important determinant on the reliability and accuracy of the solution. Because of the early adaptation of CFD in the field of congenial cardiac surgery as a tool to guide operative technique and evaluate hemodynamic and physiological consequences, we have chosen three representative cases of palliative operations for congenital heart defects (CHD) as the clinical problem to achieve our investigative objectives.

To highlight the importance of the different steps in the cardiovascular modeling process, we first summarize the main steps in the Methods section. Previously, we have demonstrated the importance of defining accurate boundary conditions [5] as a prerequisite for accurate simulation. We also note the recent review on considerations for the numerical modeling of the pulmonary, especially on hypertension, which focuses primarily on the geometry reconstruction and on boundary conditions [21]. Therefore, in this study, the focus is on mesh generation and choice of numerical methods to solve the equations governing blood flow and pressure in the region of interest and the resulting impact on clinically relevant parameters derived from the simulation. These concepts are illustrated in the results section with increasing complexity, from the simplest example of a blood flow through a rigid tube, to realistic cases in the context of single ventricle palliations. In each case, the results from two different numerical codes are compared. The results are then discussed to draw conclusions on the main points medical researchers should be aware of for numerical analysis of blood flow.

2. Methods

Blood flow numerical simulations involve, at a minimum, three steps following reconstruction of the three-dimensional (3D) geometry from cross-sectional imaging data: (1) geometrical mesh generation, (2) choice of boundary conditions for the blood flow mass and momentum balance equations, and (3) numerical computation of the solution. We recall here only what is necessary to understand the essence of each step. For more detailed description, please refer to previous publications [5,22]. These steps each have significant influence on the results and must thus be carried out with care, as will be shown in the results. The schematic in the appendix summarizes the main concepts.

2.1. *Discretization of the geometry: mesh generation*

The 3D geometry of the vessels of interest can be drawn with CAD softwares or in case of patient-specific cases, reconstructed from imaging data such as magnetic resonance angiography (see examples in Fig. 1). In most geometries and flow conditions, the mathematical, or exact, solution to the flow equations cannot be found analytically, that is, by hand or simple calculations. Hence, the solution must be approximated by breaking down the equations in time and space in such a way that the computed solution is as close as possible to the mathematical solution. Despite being approximate, the computed solution can approach the exact solution if the simulation is carried out sensibly and correctly. This defines an algorithm that computes the solution numerically over successive time steps at a finite number of locations in the blood vessels. The 3D geometry is thus discretized into small "volumes" or "elements" (tetrahedra, hexahedra, and so forth) defined by nodes (or connection points of each element) where the solution is computed (Figs. 2 and 6). The ensemble

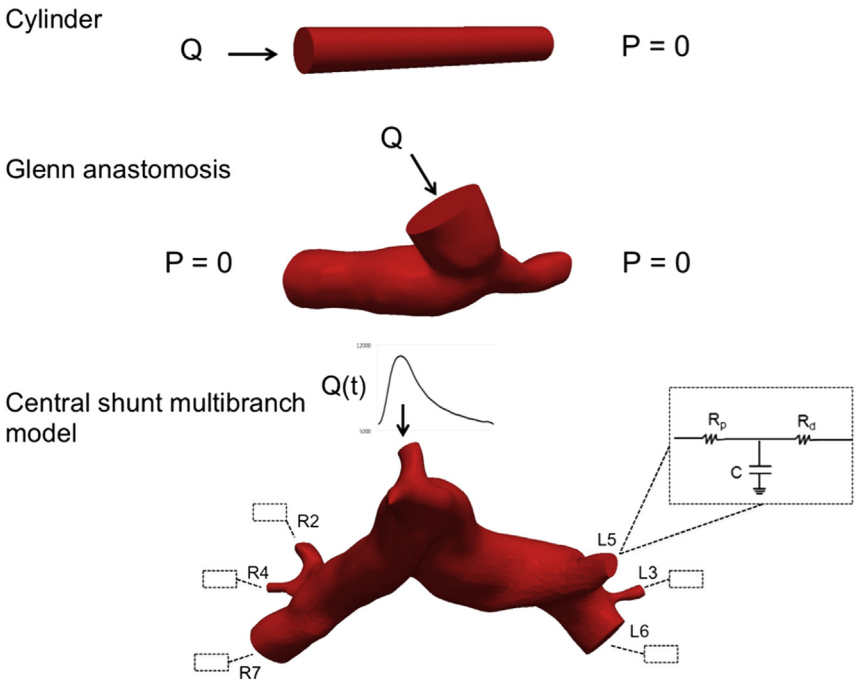

Fig. 1 – Examples of increasing geometrical (red) and physiological (inlet flow Q, outlet constant reference pressure, P_{ref}, or Windkessel boundary condition) complexity. Zero velocity is imposed on the vessel walls. Top: cylinder for which the solution is known. Middle: simple patient-specific case. Bottom: realistic patient-specific configuration. (Color version of figure is available online.)

of volumes or elements and nodes constitutes the mesh that thus represents the 3D geometry. The more elements a mesh contains, the finer the solution is. The disadvantage of mesh refinement is, however, the increase in computational cost: for instance, when the number of volumes or elements is doubled and the same computational power is used, the computational time can increase up to 10×, translating to simulations that may last several days or weeks. Mesh adaptation is a way to obtain a higher accuracy mesh, yet keep the number of elements, and thus the simulation time, reasonable [23]. This is particularly important for challenging patient-specific simulations, where blood flow shows complex structures and for geometries with disparate length scales. The geometry is first discretized into an isotropic (i.e., uniform in all orientations) mesh. An initial simulation is performed, producing a metric of local flow gradients. An anisotropic, that is, with a preferential refinement orientation, mesh is then created by adaptively placing elements in areas of high-velocity gradient that need better refinement. These steps can be repeated a number of times to increase the quality of the mesh until the desired level of accuracy is reached. Here the isotropic and anisotropic meshes were generated using tetrahedral elements with the mesh generation software MESHSIM (Simmetrix Inc, Clifton Park, NY) [23,24] except for one isotropic hexahedral element mesh, which was generated with GAMBIT (ANSYS Inc, Canonsburg, PA).

2.2. *Solved equations and boundary conditions*

Pressure and velocity are computed as solutions in space and time to the Navier-Stokes equations, which solve for the majority of the real-world fluid flow problems by assuming blood behaves as a Newtonian (viscosity: 0.004 Pa s), incompressible fluid (density: 1060 kg/m^3). These partial differential equations necessitate that appropriate boundary conditions are prescribed on the whole boundary. The vessel walls are assumed to be rigid, and a zero velocity no slip boundary condition is thus imposed there. On the inflow boundary, velocity is prescribed: in this study, it is assumed perpendicular to the surface, following a given steady (average behavior) or pulsatile (taking into account cardiac or respiratory variations) flow rate. At the outflow boundaries, one may impose a pressure (or traction) value or a simplified representation of the downstream vascular trees (here with a Windkessel model). For more information about typical boundary conditions, how they relate to physiological or patient-specific data, see the review Vignon-Clementel *et al.* [5] and references therein or more recently [2] and for related numerical issues [25].

2.3. *Flow solver numerical methods*

As mentioned above, the governing equations must be discretized in time and space in such a way that the computed solution is as close as possible to the exact solution. Finite volumes and finite elements are two families of space discretization methods, within whom many variants exist for the Navier-Stokes equations [26,27]. In addition, different schemes have been developed to march the solution in time. These choices depend on the trade-off between ease of implementation, computational cost, stability, and accuracy of the computed solution. This trade-off needs to be evaluated for each application, accounting for values of blood density

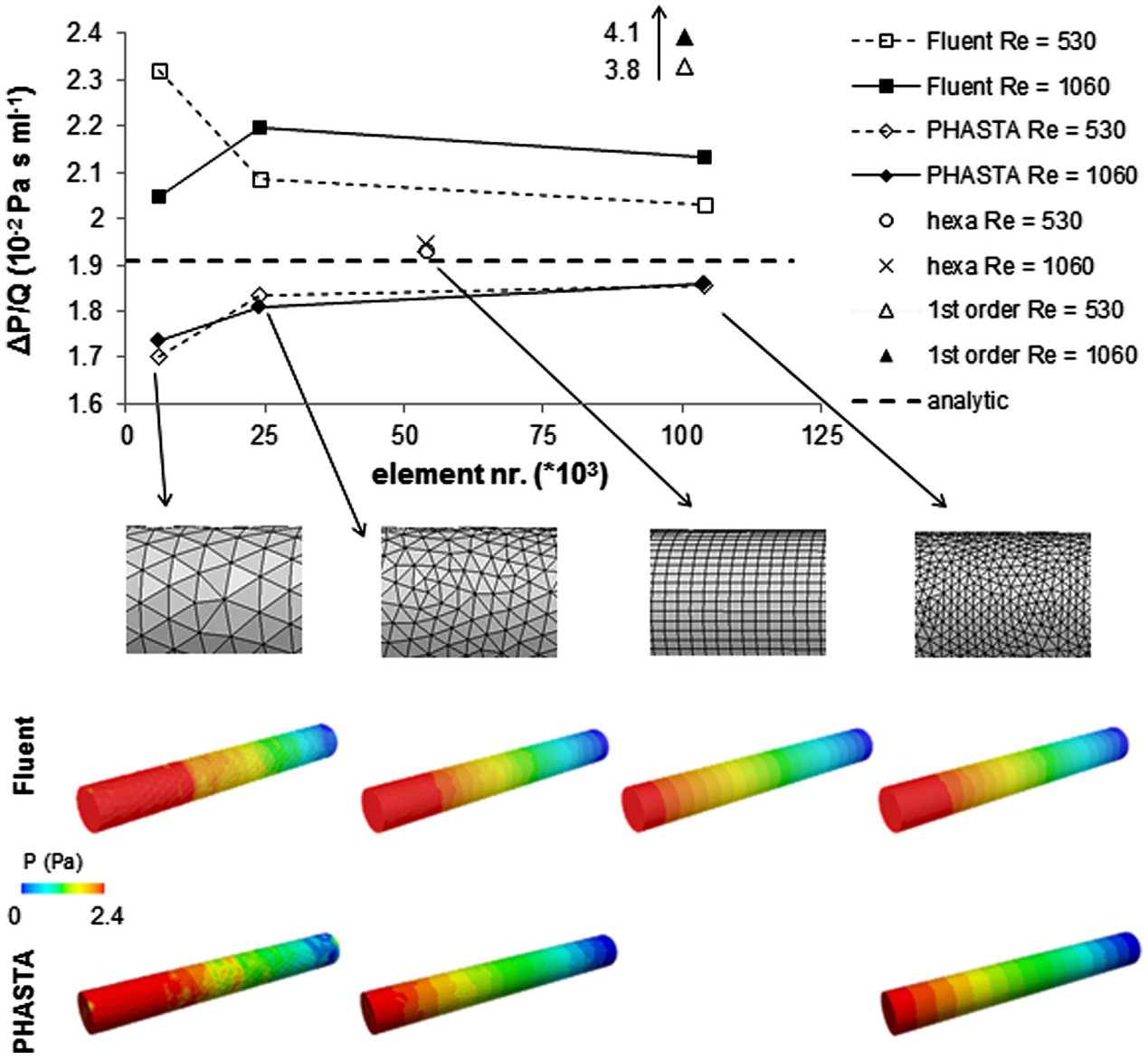

Fig. 2 – (Upper panel) Mesh convergence results shown as resistance (ΔP/Q) computed with the solution of meshes of increasing size (shown below). The dashed straight line corresponds to the analytical Poiseuille resistance. The upper curves correspond to ANSYS Fluent solutions, whereas the lower ones to PHASTA solutions, for both simulated Re. Solutions of Fluent hexahedral mesh and Fluent first-order method are also reported. (Lower panel) Pressure (Pa) maps corresponding to the different meshes computed with Fluent (top) and PHASTA (bottom), for the case with Re = 1060.

and viscosity, flow rates and pressure ranges, complexity of the flow, and precision needed to answer the medical question of the study.

In this article, we highlight how this can be done numerically, with examples of increasing complexity. In each example, two codes are compared: the commercial code ANSYS Fluent and the code PHASTA, the flow solver within the open-source software package Simvascular (www.simtk.org) [28].

Although both codes require mesh discretization to solve the fluid dynamics problem, they adopt different numerical solution methods: Fluent is based on a finite-volume scheme, whereas PHASTA uses the finite-element method. Moreover, being a general purpose CFD code, Fluent provides various numerical options and models to solve problems of different nature (e.g., laminar, turbulent, diffusion, heat transfer) and in different fields (e.g., biomechanics, energetics, aerospace, chemistry). For example, first-order or second-order approximations can be chosen for both spatial and time discretization of the Navier-Stokes equations: the former is usually faster to reach convergence of the solution, although with lower precision than the latter. If such options are not known in detail or the default settings are used, they may lead to inappropriate and risky choices. As an example, first order is the default option in Fluent, but it is usually inappropriate for most cardiovascular CFD problems. PHASTA, instead, is an in-house code specifically designed for solving complex CFD problems,

thus using numerical options (e.g., second-order approximation in time) already optimized for such problems. Open source and in-house solvers such as this offer the advantage of greater user control over numerical scheme and flexibility to implement new capabilities. Solutions from the two codes are visualized at each mesh element (Fluent) or node (PHASTA) with the software Paraview (www.paraview.org).

2.4. Setup of the three examples

A summary of the geometry and boundary conditions is explained in Figure 1 for each example of increasing complexity.

2.4.1. Simple "SVC" tube with Poiseuille flow

The conditions in the first example are representative of a superior vena cava (SVC) in an adult CHD patient, simplified enough so that an exact solution can be calculated, the well-known "Poiseuille flow." The geometry is a cylinder of radius 2 cm and length 30 cm. Three unstructured tetrahedral meshes of increasing refinement were tested (6×10^3, 2.4×10^4, and 10^5 elements), as well as a hexahedral mesh of 5.4×10^4 elements oriented along the direction of flow. Two different steady flow regimes were tested, with a Reynolds number (Re) of 530 and 1060, that is, with lower and higher flow rates, respectively. The corresponding flow was imposed at the inlet, with a parabolic axial velocity profile. In all simulations, zero velocity at the wall and a constant reference pressure at the outlet were imposed. Calculated pressures were then interpreted as differences with respect to the reference value. As a consequence, the mathematical solution is, in this simple case, analytically known and can be compared with the numerical solutions. It is the Poiseuille solution, with a parabolic axial velocity solution that is constant along the length of the cylinder, and a pressure solution which is uniform on a given cross-sectional area but decays linearly along the length of the cylinder. The resistance to flow, which is the ratio of the pressure loss along the tube divided by the flow, can then be compared between the analytical and the numerical solutions.

2.4.2. Steady superior cavopulmonary connection, or Glenn anastomosis, model

As the second stage palliation for single ventricle hearts, the SVC is disconnected from the right atrium and connected directly to the pulmonary artery to provide pulmonary blood flow. Contrary to the previous case, the exact solution of the flow equations in a Glenn anastomosis cannot be derived analytically, due to its complex geometry and flow characteristics and compulsory three-dimensionality. To compare the differences between codes and between meshes is thus more difficult as the mathematical exact solution is unknown. The SVC anastomosis to the left pulmonary artery and right pulmonary artery (RPA) was reconstructed from magnetic resonance imaging data of a single-ventricle patient following the Glenn operation. The SVC averaged diameter is 12.2 mm. In this example, only the geometrical complexity is increased to see its influence on the solution in the simplest hemodynamics setting. Steady flow (2.6×10^{-5} m^3/s) with a flat axial velocity profile was imposed at the inlet (SVC), zero flow at the wall, and the same reference pressure at the outlets. It is worth noting that, with rigid-walled models, CFD results are identical regardless of which value is used as a reference. In this case, it would be obvious to use a reasonable value for mean pulmonary artery pressure, but zero pressure could be indifferently applied, without affecting the solution in terms of flow distribution and pressure gradients. A uniform mesh was created (2.4×10^5 elements, indicated as "240 K") and adapted first with 5.4×10^5 elements and then with 1.4×10^6 elements (indicated as "1.4 M").

2.4.3. Pulsatile multidomain central shunt pulmonary model

This case presents a realistic and patient-specific simulation for both geometry and physiology (Fig. 1). Constructed from magnetic resonance imaging data, the geometry consists of a systemic to pulmonary shunt connected between the aorta and the PA as the first stage of single ventricle palliation. The inlet shunt flow was imposed with typical cardiac pulsatility (as measured by ultrasound) for several cardiac cycles, with a flat velocity profile. The average flow was 7.5×10^{-6} m^3/s (corresponding to an average inlet Re of about 10^3). To model the pressure drop-flow relationship of the pulmonary arterial trees downstream of the outlets, three-element Windkessel models, each composed of a proximal resistor in series with a capacitor and a distal resistor in parallel, are coupled to these outlets. Proximal and distal resistances represent the viscous effects of blood flowing through the pulmonary arterial and capillary-venous bed, respectively, whereas the capacitance accounts for vessel wall deformability. The distal pressure was taken as the average atrium pressure (6 mmHg). The parameters can be automatically tuned based on the magnetic resonance left/right pulmonary flow split, catheter-based transpulmonary gradient, diameter of each outlet, and morphometric data. This method allows one to obtain realistic pressure and flow values [2]. The mesh was first adapted in a steady simulation from a 5×10^6 isotropic element mesh to an anisotropic 2.7×10^6 element mesh and then further adapted in a pulsatile simulation to an anisotropic 1.9×10^6 element mesh, with a target error reduction of 20% each time [23]. The maximum values did not change between the two last meshes, and the flow structures were very similar. The time step was 0.001 s and two cycles were enough to reach stable waveforms.

3. Results

3.1. Simple tube with Poiseuille flow

The simulation results were compared for the different meshes and codes (Fig. 2, upper panel). In general, the results get closer to the analytical exact solution as the mesh is refined. ANSYS Fluent overestimates the resistance, whereas PHASTA underestimates it, regardless of flow rate; but both codes converge to the analytical solution. The convergence to the analytical solution is faster for low flow (Re = 530) than for high flow (Re = 1060). Note that for higher flow, the coarsest

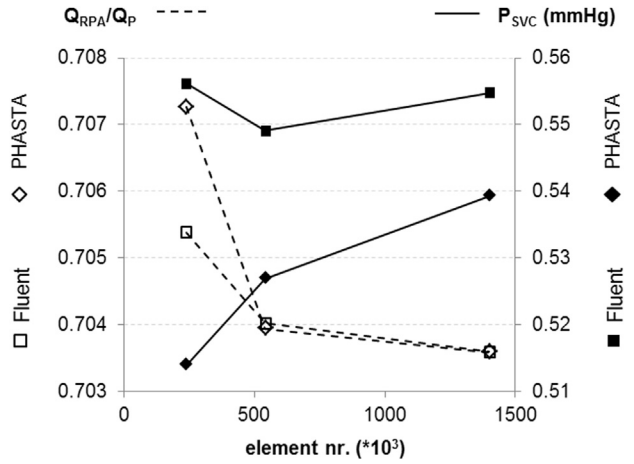

Fig. 3 – Numerical solution computed with PHASTA (diamonds) and ANSYS Fluent (squares). Flow split (Q_{RPA}/Q_P) to the right PA (left axis, open symbols) and SVC inlet pressure (in mmHg, right axis, filled symbols) for meshes of increasing refinement (number of elements on x-axis). 1 mmHg = 133 Pa.

mesh (6×10^3 element mesh noted 6k) run with ANSYS Fluent appears to be closer to the analytical solution for the resistance. However, the pressure map (Fig. 2, lower panel, top left) reveals that the pressure is spotty and not linearly decreasing, contrary to the analytical solution. This is also the case for the 6k-mesh PHASTA simulation (Fig. 2, lower panel, bottom left). This stresses the importance of selecting a relevant criterion to assess mesh convergence.

One way to construct a mesh that provides a better solution, while limiting the number of elements, is to align the elements with the flow. In this simple unidirectional flow, a hexahedral mesh is particularly well suited: the 54k element-mesh, which has about half the number of nodes compared with the finer mesh, leads to a solution much closer to the analytical solution (Fig. 2, upper panel for the resistance value and lower panel top for the linear pressure decay with Re = 1060).

Moreover, selecting the " first-order method" as a numerical discretization method in ANSYS Fluent lead to a pressure drop double the analytical solution (Fig. 2, upper panel).

3.2. *Steady Glenn anastomosis model*

To show the influence of mesh refinement, a mesh comparison was performed with three increasingly refined meshes, and the differences between codes were compared (Fig. 3).

The SVC pressure for PHASTA is going toward an asymptote with about 2% increase (corresponding to about 0.01 mmHg) when refining the mesh (i.e., more than doubling the number of elements at each adaptation). On the other hand, with Fluent, it oscillates around a value (about 0.55 mmHg) with changes of around 1% (corresponding to about 0.005 mmHg). For both solvers, the flow split between the two pulmonary arteries (PAs) quickly converges to the same value (0.703).

The 3D pressure (Fig. 4) and velocity (Fig. 5) maps demonstrate minimal differences between the two solvers' solutions. Moreover, the maps confirm that the differences between meshes are minimal and that the coarsest mesh (240 K) is thus appropriate for this type of geometry and flow conditions.

The mesh has adapted to the flow structures, creating a boundary layer at the SVC inlet, where a flat flow profile was imposed, and a swirling pattern on the RPA outlet section (Fig. 6), where the flow swirls.

Note that the computed flow split shows a right dominance. This is a consequence of applying an equal pressure at the two outlets and a larger RPA diameter. However, if the flow split is measured clinically (e.g., by phase-contrast magnetic resonance imaging), the boundary conditions should incorporate this data, for example, directly imposing the outflows or setting downstream resistances such that the measured flow split is obtained. Furthermore, taking into account unsteadiness has been shown to influence the results (due to nonlinear effects) [29].

3.3. *Pulsatile multiscale central shunt pulmonary model*

In this realistic multibranched model, the aforementioned limitations are alleviated. Results are shown as velocity cuts and pressure maps on the final adapted mesh (1.9×10^6 elements) at end diastole and peak systole (Fig. 7). They illustrate how complex the hemodynamics are in such an anatomy. Blood enters at high speed through the shunt (Fig. 7A) and impacts the pulmonary wall (red

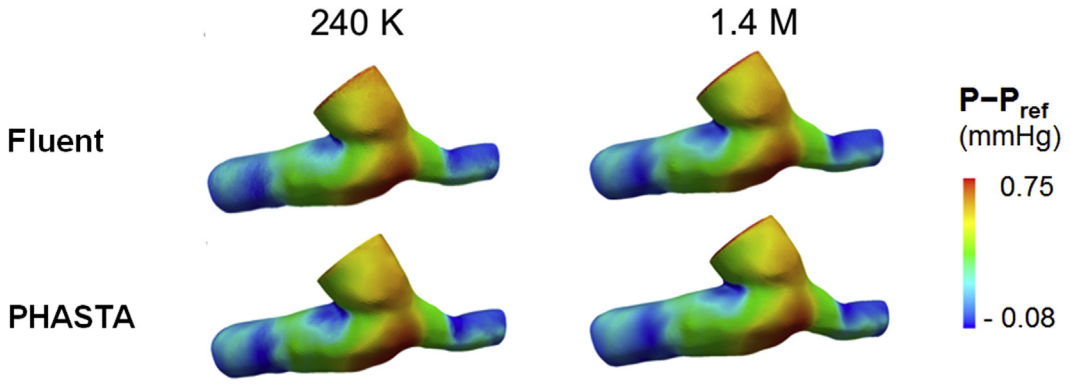

Fig. 4 – Pressure (mmHg) maps for meshes with 240 K (left) and 1.4 M (right) elements, computed with Fluent (top) and PHASTA (bottom). Depicted pressure is relative to the reference pressure, P_{ref}, applied to the models outlets.

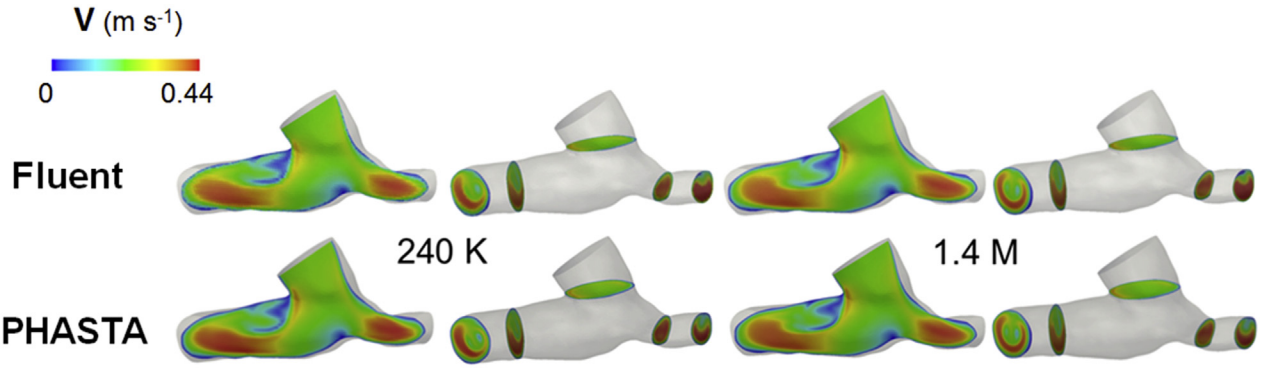

Fig. 5 – Velocity magnitude (m/s) cuts for meshes with 240 K (first two columns on the left) and 1.4 M (last two columns on the right) elements, computed with Fluent (top) and PHASTA (bottom).

in Fig. 7C), causing a high-pressure region (circular patches on the right of the main pulmonary artery stump in Fig. 7B). Blood swirls downstream into the PAs (cyan structures in Fig. 7C and D).

The interaction between the 3D geometry and the high flow in the narrow shunt spreading into the PAs generates flow dynamics that are not completely periodic over time. This is reflected by the flow and pressure tracings over time at two outlets Figure 8.

Because this case includes 3D model characterized by multiple pulmonary branches and relatively high inlet velocity, generating complex fluid dynamics, it is interesting to compare the two codes in terms of flow distribution at the outlets and of local velocities and pressures. The Table shows, for the two solvers, how closely flow rates and pressures match at the outlets, on average over time, with relative differences <2.4%. The comparison of pressure and velocity maps shows that the results are very similar between the two solvers, at low (end diastole) and high (peak systole) flows: both of them detect flow impingement on the pulmonary wall at the exit of the shunt, with local maximal velocity values (3.5 m/s in Fig. 7C), and swirling flow in the PAs. Note that the maximum pressure actually occurs not at the inlet but at the impingement on the pulmonary wall, where the two codes computed the same value (76 mmHg; Fig. 7B).

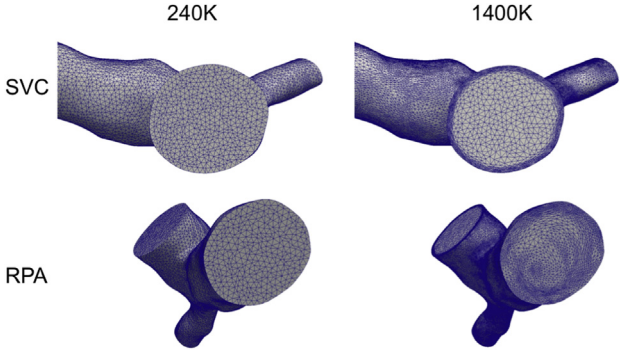

Fig. 6 – Uniform initial mesh (240 K elements) and refined mesh (1.4 M elements) that adapted to the flow structures, as shown at the inlet (SVC), where a flat profile is imposed, and at the largest outlet (RPA), where the flow swirls. (Color version of figure is available online.)

4. Discussion

The first example (simple tube with Poiseuille flow) illustrates that, even for a simple Poiseuille flow, selecting the mesh impacts the results. Here the hexagonal mesh leads to better results: this mesh is the most axisymmetric and aligned with the flow among all the other meshes. To generalize this observation to more complex geometries and flows is the subject of another study. The better suitability of hexagonal *versus* tetrahedral meshes is a matter of debate in fluid mechanics [30] that is beyond the scope of this article. However, the results do highlight that the fineness of the mesh should be determined based on the relevant output: taking into account just a global measure rather than local phenomena may be misleading. It is thus necessary to define a convergence criterion to assess when to stop the mesh refinement.

The chosen level of refinement depends on the flow conditions and numerical methods of the code at hand. The first-order method on a fine mesh in Fluent, which is the default and faster method, had a 100% error in the pressure drop. This is likely due to the added energy dissipation to achieve numerical stability of the numerical method. This stresses the importance of testing the numerical method according to the application. The mesh can, however, be refined anisotropically based on how the blood flows, to keep the computational time reasonable while improving the solution quality.

Indeed, in the second example (steady Glenn anastomosis model), appropriate mesh adaptation was performed. However, the results show that for these meshes and simple hemodynamic conditions, the mesh had little impact on the SVC pressure and the flow split between the two lungs. Changes in the SVC pressure of about 2% for PHASTA and 1% for Fluent (Fig. 4) are clinically negligible because they correspond to very small fractions of mmHg (about 0.01 and 0.005 mmHg, respectively). Changes in flow split with mesh refinement are even slighter if compared with SVC pressure.

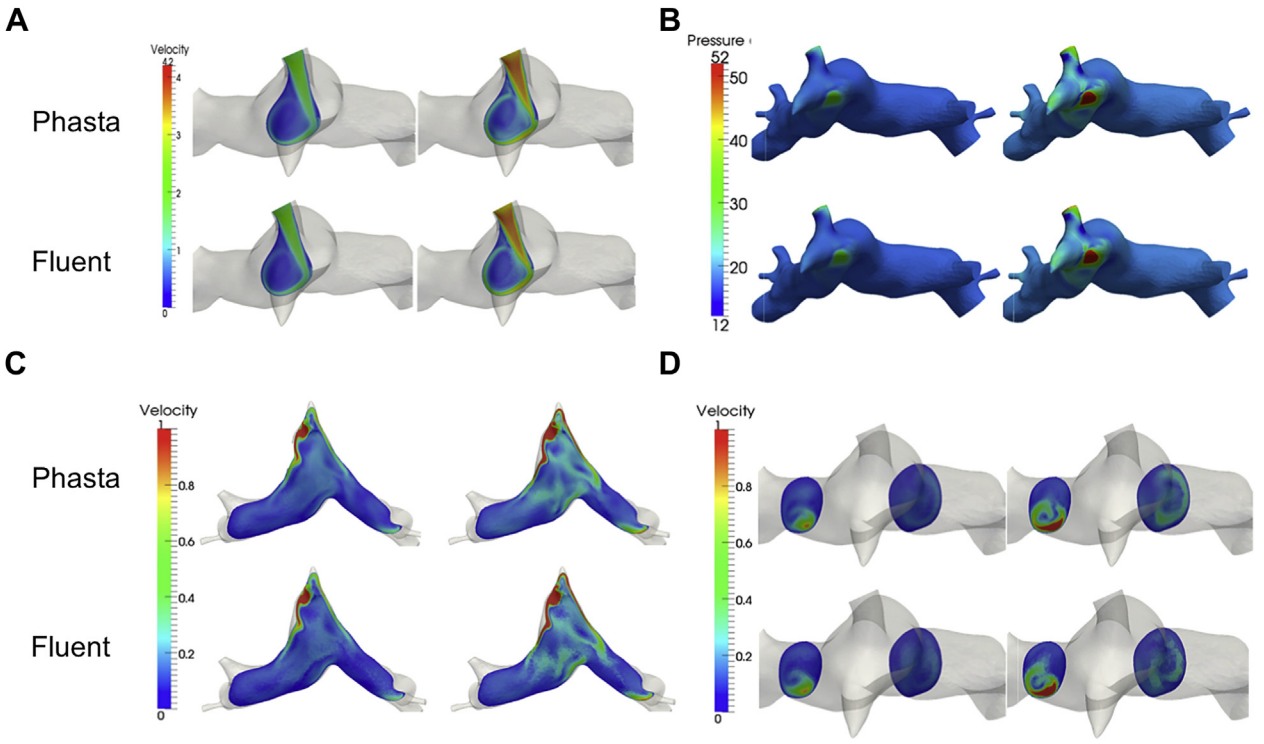

Fig. 7 – Comparison between the two codes (PHASTA and Fluent) of pressure (mmHg) (B) and velocity magnitude (m/s) at the anastomosis (A), on an axial cut (C) and on sagittal cuts through the pulmonary arteries (D), in end diastole (first and third columns) and peak systole (second and fourth columns). The maximum legend values were chosen as a compromise between showing the high values and visualizing flow and pressure structures.

The 3D maps (Figs. 5 and 6) confirm this point. The first mesh is thus fine enough for these conditions and these convergence criteria.

The difference between the codes, although very small compared with pressure measurement uncertainties, decreases with the refinement of the mesh: for the SVC pressure, it decreased from 8% to 4% and then to 3%. Note that in this case, the "true" solution is not known, so it can only be obtained by such a convergence study. From a practical point of view, the appropriate refinement is defined by metrics that depend on the purpose of the hemodynamic simulations, for example, pressure drop, flow repartition, or finer information such as wall shear stress, which usually requires a significant increase in mesh quality.

The third example adopting solution to a pulsatile multidomain central systemic pulmonary shunt is a simulation with realistic geometry and physiological conditions. The mesh was adapted to the solution. The complexity of the flow and the associated effects on pressure distribution were captured by both codes. This observation is noteworthy from a clinical perspective, as complex hemodynamics with increased turbulence, increased particle residence time, and abnormal shear stresses may have important impact on

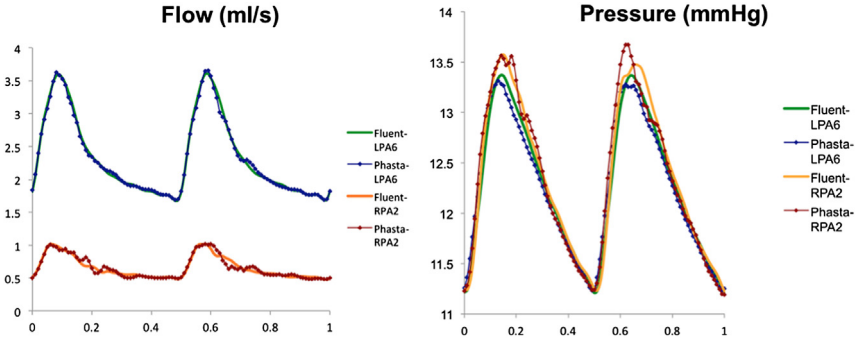

Fig. 8 – Comparison of flow (left) and pressure (right) over time (in seconds) at one small branch on the RPA and one large branch on the LPA, between the two codes (Fluent, lines; PHASTA, dotted lines). (Color version of figure is available online.)

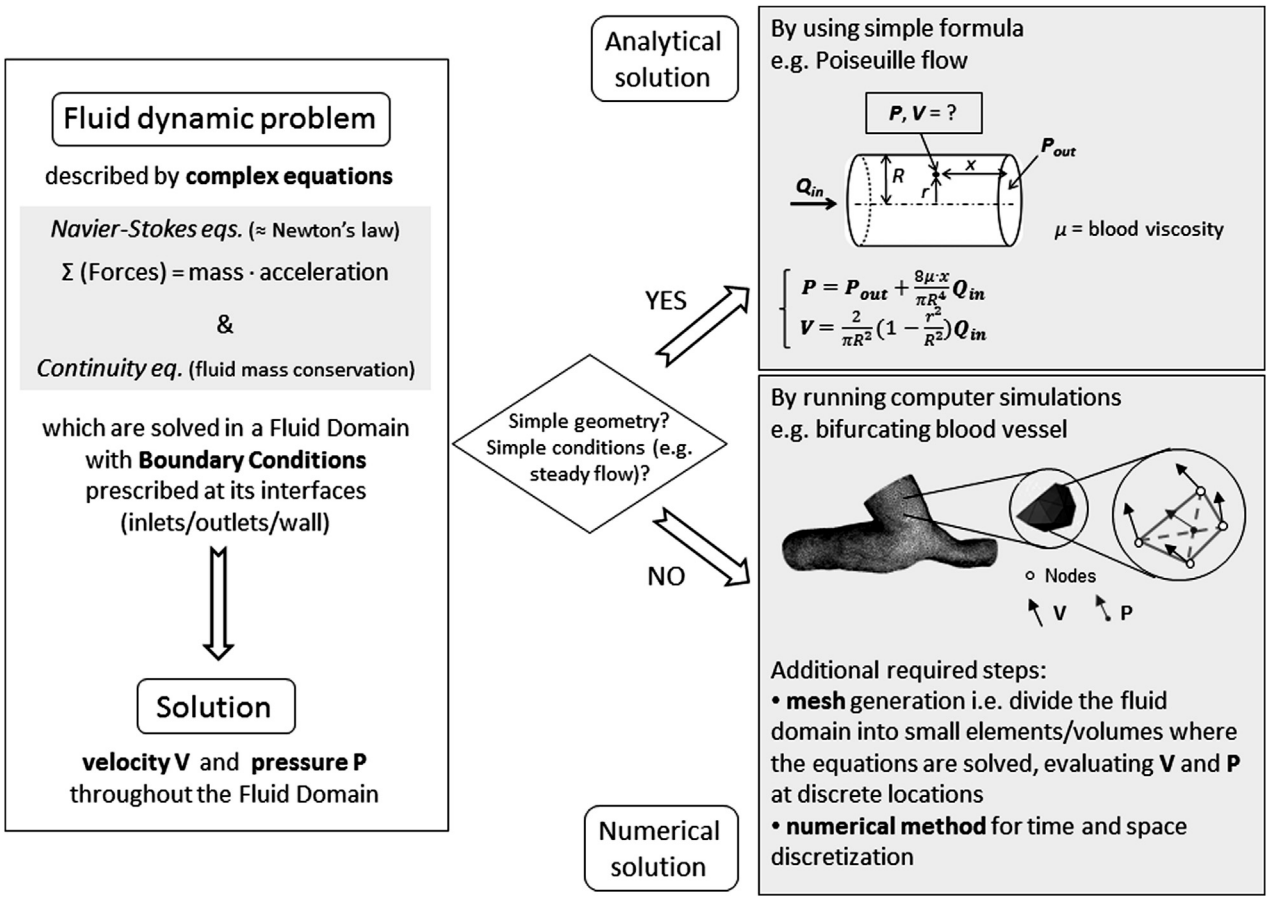

Fig. 9 – Schematic summarizing key basic concepts for readers with little numerical background.

potential for thromboembolic phenomenon, flow distribution to the right and left lungs, and vascular wall remodeling. The solutions over time and in space were largely similar. It is thus expected that the chosen numerical methods for each code would give comparable differences on similar patient-specific hemodynamics simulations.

Another consideration in choosing a CFD method is the overall computational time. In fact, the latter may vary according to time and space discretization methods, the mesh size, the programming language, the computing power at hand, and so forth. As with the mesh refinement study, a time-step refinement study should be performed. In both cases, there is a tradeoff between computational cost and accuracy of the solution. Reducing computational complexity is yet a matter of intense research.

One factor that increases computational time but may be necessary for some applications is to take into account the elastic or viscoelastic nature of the vessel walls when solving the blood flow equations. To take into account such a fluid-solid interaction necessitates proper algorithms (e.g., [31,32]) and additional modeling parameters to select or estimate from patient data [33]. As for boundary conditions, such choices need to be consistent with the clinical question being addressed and the patient data or population data available in the literature [5].

Other considerations may also drive the choice of flow solvers. Commercial solvers are designed to be easier to use, with intuitive user-interfaces and training courses. This facilitates the entrance into the simulation field for new users. In traditional engineering applications, these codes have been tested in R&D companies in the context of product design. In cardiovascular research, the CFD community is still growing, with a wide spectrum of CFD conditions, ranging for low Re flow in small animals [34] to near-turbulent flow in patient congenital or acquired diseases [3,35]. For each application, numerical methods need to be tested. In fact, the interaction of patient-specific 3D multibranched geometry and the hemodynamics conditions can create a highly complex flow, with unsteady swirling structures that are far from unidirectional

Table – Time average pressure and flow at the six branches.

Branch name	R2	L3	R4	L5	L6	R7
Pressure (mmHg)						
PHASTA	12.37	11.94	12.69	12.28	12.26	12.32
Fluent	12.35	11.95	12.53	12.29	12.28	12.32
Flow (mL/s)						
PHASTA	0.659	0.120	0.176	0.299	2.326	3.914
Fluent	0.659	0.120	0.172	0.300	2.330	3.910

flow. This can cause numerical challenges for which traditional approaches, found in commercial codes, sometimes fail. Specific numerical methods are, in such cases, warranted and implemented in in-house research codes [36]. Moreover, in hemodynamics simulations, the 3D region of interest is part of the global circulation. To take into account the interaction between the local hemodynamics effects and the rest of the circulation, the 3D hemodynamics equations can be coupled to reduced models (e.g., lumped parameter models [6,37–41]) of the entire circulation instead of just a Windkessel model as was done here. Such a coupling can be numerically challenging. Commercial codes offer limited possibilities to do it, whereas in-house codes, with more developmental work, can be tailored for efficiency and robustness [25,42,43]. For example, in commercial codes, the reduced model can be coupled to the 3D domain with a user-defined routine. But the coupling is done explicitly in time, which requires using a smaller time-step size to maintain numerical stability and thus longer simulation times.

5. Conclusion

The "take home points" are summarized in the Appendix table for readers less familiar with CFD numerical tools. Even in very simple fluid dynamics conditions (Poiseuille flow), expertise and careful numerical choices are mandatory to obtain a robust and accurate solution. At least a basic numerical knowledge is thus required to appropriately use codes or formulas [5,44]. For example, a mesh sensitivity study is warranted, based on a chosen convergence criterion, usually a threshold of change in an output quantity, that depends on the accuracy necessary for the medical question at hand. Other choices are important in addition to the number or the location of the elements: element shape (hexahedra *versus* tetrahedra) and numerical schemes (time and space discretization methods). These choices depend on both the hemodynamic conditions (low flow or high flow, interaction with more or less complex geometry) and the output relevant for the application. In fact, meshes and numerical parameters chosen for simulations under resting conditions may not be appropriate for exercise conditions. Similarly, to evaluate a pressure loss may require less restrictive numerical parameters than to capture 3D flow features or wall shear stress. Finally, with the present study, we underlined that the choice of proper numerical settings is more important than the solver (code) choice [20].

Acknowledgment

This work was supported by a Leducq Foundation Network of Excellence Grant, a Burroughs Wellcome Fund Career Award at the Scientific Interface, and an INRIA associated team program. We gratefully acknowledge the use of software from the Simvascular open source project through Simbios (http://simtk.org).

REFERENCES

[1] Yeung JJ, Kim HJ, Abbruzzese TA, et al. Aortoiliac hemodynamic and morphologic adaptation to chronic spinal cord injury. J Vasc Surg 2006;44:1254. e1251.
[2] Troianowski G, Taylor CA, Feinstein JA, Vignon-Clementel IE. Three-dimensional simulations in Glenn patients: clinically based boundary conditions, hemodynamic results and sensitivity to input data. J Biomechanical Engineering-Transactions Asme 2011;133:111006.
[3] LaDisa JF Jr, Dholakia RJ, Figueroa CA, et al. Computational simulations demonstrate altered wall shear stress in aortic coarctation patients treated by resection with end-to-end anastomosis. Congenit Heart Dis 2011;6:432.
[4] Torii R, Oshima M. An integrated geometric modelling framework for patient-specific computational haemodynamic study on wide-ranged vascular network. Computer Methods Biomech Biomed Eng 2011;15:615.
[5] Vignon-Clementel IE, Marsden AL, Feinstein JA. A primer on computational simulation in congenital heart disease for the clinician. Prog Pediatr Cardiol 2010;30:3.
[6] Corsini C, Baker C, Kung E, et al. An integrated approach to patient-specific predictive modeling for single ventricle heart palliation. Comput Methods Biomech Biomed Engin. 2013 [Epub ahead of print].
[7] Hsia TY, Cosentino D, Corsini C, et al. Use of mathematical modeling to compare and predict hemodynamic effects between hybrid and surgical Norwood palliations for hypoplastic left heart syndrome. Circulation 2011;124:S204.
[8] Yang W, Vignon-Clementel I, Troianowski G, Reddy V, Feinstein J, Marsden A. Hepatic blood flow distribution and performance in conventional and novel Y-graft Fontan geometries: a case series computational fluid dynamics study. J Thorac Cardiovasc Surg 2012;143:1086.
[9] Kung E, Baretta A, Baker C, et al. Predictive modeling of the virtual Hemi-Fontan operation for second stage single ventricle palliation: two patient-specific cases. J Biomech 2013;46:423.
[10] Moghadam ME, Migliavacca F, Vignon-Clementel IE, Hsia TY, Marsden AL. Optimization of shunt placement for the Norwood surgery using multi-domain modeling. J Biomech Eng 2012;134:051002.
[11] Morales HG, Kim M, Vivas EE, et al. How do coil configuration and packing density influence intra-aneurysmal hemodynamics? Am J Neuroradiology 2011;32:1935.
[12] Koo BK, Erglis A, Doh JH, et al. Diagnosis of ischemia-causing coronary stenoses by noninvasive fractional flow reserve computed from coronary computed tomographic angiograms. Results from the prospective multicenter DISCOVER-FLOW (Diagnosis of Ischemia-Causing Stenoses Obtained Via Noninvasive Fractional Flow Reserve) study. J Am Coll Cardiol 2011;58:1989.
[13] Prasad A, To LK, Gorrepati ML, Zarins CK, Figueroa CA. Computational analysis of stresses acting on intermodular junctions in thoracic aortic endografts. J Endovasc Ther 2011; 18:559.
[14] Pant S, Limbert G, Curzen NP, Bressloff NW. Multiobjective design optimisation of coronary stents. Biomaterials 2011; 32:7755.
[15] Yang W, Feinstein JA, Shadden SC, Vignon-Clementel IE, Marsden AL. Optimization of a y-graft design for improved hepatic flow distribution in the fontan circulation. J Biomech Eng 2013;135:011002.
[16] Stewart S Computer methods in cardiovascular device design & evaluation: overview of regulatory best practices. Computer methods for cardiovascular devices: a workshop sponsored by FDA/NHLBI/NSF. Bethesda, MD, USA: 2008.

http://www.fda.gov/scienceresearch/specialtopics/criticalpathinitiative/spotlightoncpiprojects/ucm149414.htm.
[17] Stewart SC, Paterson E, Burgreen G, et al. Assessment of CFD performance in simulations of an idealized medical device: results of FDA's First Computational Interlaboratory Study. Cardiovasc Eng Technology 2012;3:139.
[18] Pekkan K, De Zelicourt D, Ge L, et al. Physics-driven CFD modeling of complex anatomical cardiovascular flows-a TCPC case study. Ann Biomed Eng 2005;33:284.
[19] Radaellia AG, Augsburger L, Cebral JR, et al. Reproducibility of haemodynamical simulations in a subject-specific stented aneurysm model—a report on the Virtual Intracranial Stenting Challenge 2007. J Biomech 2008;41:2069.
[20] Steinman DA, Hoi Y, Fahy P, et al. Variability of computational fluid dynamics solutions for pressure and flow in a giant aneurysm: the ASME 2012 Summer Bioengineering Conference CFD Challenge. J Biomechanical Eng 2013;135:021016.
[21] Kheyfets VO, O'Dell W, Smith T, Reilly JJ, Finol EA. Considerations for numerical modeling of the pulmonary circulation—a review with a focus on pulmonary hypertension. J Biomech Eng 2013;135:61011.
[22] Taylor CA. Figueroa CA patient-specific modeling of cardiovascular mechanics. Annu Rev Biomed Eng 2009;11:109.
[23] Sahni O, Muller J, Jansen KE, Shephard MS, Taylor CA. Efficient anisotropic adaptive discretization of the cardiovascular system. Computer Methods Appl Mech Eng 2006;195:5634.
[24] Müller J, Sahni O, Li X, Jansen KE, Shephard MS, Taylor CA. Anisotropic adaptive finite element method for modelling blood flow. Computer Methods Biomech Biomed Eng 2005;8:295.
[25] Esmaily Moghadam M, Vignon-Clementel IE, Figliola R, Marsden AL. A modular numerical method for implicit 0D/3D coupling in cardiovascular finite element simulations. J Comput Phys 2013;244:63.
[26] Gresho PM, Sani RL. Incompressible flow and the finite element method. Wiley; 2000.
[27] Eymard R, Gallouet T, Herbin R. Finite volume methods. In: Ciarlet PG, Lions JL, editors. Techniques of Scientific Computing, Part III, Handbook of Numerical Analysis. Vol. VII. North-Holland: Amsterdam; 2000. p. 713—1020.
[28] Schmidt JP, Delp SL, Sherman MA, Taylor CA, Pande VS, Altman RB. The Simbios National Center: Systems Biology in Motion. Proc IEEE Inst Electr Electron Eng 2008;96:1266.
[29] Marsden A, Vignon-Clementel I, Chan F, Feinstein J, Taylor C. Effects of exercise and respiration on hemodynamic efficiency in CFD simulations of the total cavopulmonary connection. Ann Biomed Eng 2007;35:250.
[30] De Santis G, Mortier P, De Beule M, Segers P, Verdonck P, Verhegghe B. Patient-specific computational fluid dynamics: structured mesh generation from coronary angiography. Med Biol Eng Comput 2010;48:371.
[31] Causin P, Gerbeau J, Nobile F. Added-mass effect in the design of partitioned algorithms for fluid-structure problems. Computer Methods Appl Mech Eng 2005;194:4506.
[32] Figueroa CA, Vignon-Clementel IE, Jansen KE, Hughes TJR, Taylor CA. A coupled momentum method for modeling blood flow in three-dimensional deformable arteries. Computer Methods Appl Mech Eng 2006;195:5685.
[33] Moireau P, Bertoglio C, Xiao N, et al. Sequential identification of boundary support parameters in a fluid-structure vascular model using patient image data. Biomech Model Mechanobiology 2013;12:475.
[34] Greve JM, Les AS, Tang BT, et al. Allometric scaling of wall shear stress from mice to humans: quantification using cine phase-contrast MRI and computational fluid dynamics. Am J Physiology-Heart Circulatory Physiol 2006;291:H1700.
[35] Les AS, Shadden SC, Figueroa CA, et al. Quantification of hemodynamics in abdominal aortic aneurysms during rest and exercise using magnetic resonance imaging and computational fluid dynamics. Ann Biomed Eng 2010;38:1288.
[36] Moghadam ME, Bazilevs Y, Hsia T-Y, Vignon-Clementel IE, Marsden AL. A comparison of outlet boundary treatments for prevention of backflow divergence with relevance to blood flow simulations. Comput Mech 2011;48:277.
[37] Lagana K, Dubini G, Migliavacca F, et al. Multiscale modelling as a tool to prescribe realistic boundary conditions for the study of surgical procedures. Biorheology 2002;39:359.
[38] Migliavacca F, Balossino R, Pennati G, et al. Multiscale modelling in biofluidynamics: application to reconstructive paediatric cardiac surgery. J Biomech 2006;39:1010.
[39] Kim HJ, Vignon-Clementel IE, Coogan JS, Figueroa CA, Jansen KE, Taylor CA. Patient-specific modeling of blood flow and pressure in human coronary arteries. Ann Biomed Eng 2010;38:3195.
[40] Blanco PJ, Feijóo RA A dimensionally-heterogeneous closed-loop model for the cardiovascular system and its applications.
[41] Baretta A, Corsini C, Marsden A, et al. Respiratory effects on hemodynamics in patient-specific CFD models of the Fontan circulation under exercise conditions. Eur J Mech B-Fluids 2012;35:61.
[42] Malossi ACI, Blanco PJ, Deparis S, Quarteroni A. Algorithms for the partitioned solution of weakly coupled fluid models for cardiovascular flows. Int J Numer Methods Biomed Eng 2011;27:2035.
[43] Leiva JS, Blanco PJ, Buscaglia GC. Iterative strong coupling of dimensionally heterogeneous models. Int J Numer Methods Eng 2010;81:1558.
[44] Yoganathan AP, Cape EG, Sung HW, Williams FP, Jimoh A. Review of hydrodynamic principles for the cardiologist: applications to the study of blood flow and jets by imaging techniques. J Am Coll Cardiol 1988;12:1344.

Appendix

Figure 9 shows a schematic summarizing key basic concepts for readers with little numerical background. In addition, these readers might find the following list useful.

Take home points for numerical model construction

- Not a simple "click of a button," no "once-and-for-all" parameters
- To make **modeling assumptions coherent** with the **biomedical question**
  - selection of physical modeled phenomena: Newtonian or not fluid, rigid *versus* elastic walls, and so forth.
  - proper **boundary conditions**, for example, avoid forcing velocity at the outlet sections, but rather prescribing a relationship between pressure and flow that reflects in a simple way the downstream circulation, first ensuring that the fluid dynamic region of interest is not too close to the outlet
- To create a good **mesh**: proper **geometry discretization** of the problem
  - mesh generation: usually tetrahedra for complex geometries (e.g., bifurcating blood vessel); hexahedra increase solution accuracy but difficult to construct
  - sensitivity analysis to choose the proper mesh density (i.e., number of elements/volumes): running simulations with increasingly finer meshes and making sure that quantities of interest do not change more than a chosen threshold (e.g., 1%–5%)
  - mesh adaptation to selectively refine the mesh (e.g., in correspondence of a stenosis, bifurcation, or sharp curvature) based on preliminary simulation results
- To select a proper **numerical method**
  - first, second, or higher order **discretization method** of Navier-Stokes and continuity equations in space and time: based on the problem complexity
  - **time step** selection: meeting requirements of the selected method (usually based on the Courant number accounting for the size of the mesh elements/volumes and on the involved velocities) and performing a sensitivity analysis to choose the proper time step for marching the solution in time
- **More important** than choosing a certain commercial or in-house code, **to test it for the specific application**